DOI: 10.1002/ejic.200900387

Inhomogeneous Magnet $NaMn^{III}[BP_2O_7(OH)_3]$: Ferromagnetic Clusters Inserted in a Metamagnetic Matrix

Tao Yang,[a] Yan Zhang,[b] and Jianhua Lin*[a]

Keywords: Manganese / Magnetic properties / Inhomogeneity / Cluster glass

$NaMn^{III}[BP_2O_7(OH)_3]$ (**1**) has been hydrothermally synthesized and characterized by single-crystal X-ray diffraction. The manganese(III) cations are coordinated in a tetragonal-elongated octahedral environment, indicating the possible large magnetic anisotropy. The MnO_6 octahedra are interconnected by BO_4/PO_4 groups, forming a 3D triclinic net of Mn^{III} backbone. Detailed dc and ac magnetic measurements have been conducted, and a preliminary *H*–*T* phase diagram is deduced accordingly. Compound **1** adopts an unusual magnetic inhomogeneous model, consisting of ferromagnetic clusters and a metamagnetic background: At the paramagnetic temperature region, the Curie–Weiss fit shows that the manganese atoms are all in the high spin state ($S = 2$), and the predominant interaction is ferromagnetic. An antiferromagnetic ground state forms at approximately 10 K, the isothermal magnetizations between 6.5 and 10 K show the typical metamagnetism. At approximately 6.5 K, a short-range ordering of the ferromagnetic cluster occurs. Below 3.5 K, the ferromagnetic clusters tend to be frozen at low external field, and the inhomogeneous magnetism can be clearly indicated by the isothermal magnetizations below 3 K. This unusual magnetism cannot be understood by the popular mechanism in doped manganese perovskites, which are well known to be magnetically inhomogeneous because of the mixed valence of manganese. In compound **1**, one of the possible reasons for this unusual behaviour is the competition between magnetic superexchange interactions and the large magnetic anisotropy of Mn^{III}.

Introduction

Magnetic inhomogeneity, the coexistence of different magnetic phases in a chemically homogeneous compound, is an interesting dynamic phenomenon in strongly correlated electron systems.[1] In doped manganese perovskites, there is growing consensus that the inability to attain a unique thermodynamic ground state is an intrinsic feature. This issue attracts a lot of attention because of the strong correlation between inhomogeneous magnetism and colossal magnetoresistance.[2] The change in the dynamic phase equilibrium with composition, temperature and applied field has been extensively studied by various methods both theoretically and experimentally.[3] In mixed-valent manganese perovskites, it is commonly accepted that the magnetic inhomogeneity, composed of nanometric-scale ferromagnetic (FM) clusters and the long-range ordered antiferromagnetic background, originates from the competition between Mn^{III}–O–Mn^{IV} double-exchange (DE) and Mn^{III}–O–Mn^{III} superexchange (SE) interactions. Most previous research is focused on the composition–temperature phase diagrams. It appears that the existence of mixed valence in manganese is indispensable. Herein, we present a novel magnetically inhomogeneous compound, $NaMn^{III}[BP_2O_7(OH)_3]$ (**1**). It shows the valent singularity of manganese but possesses an unusual magnetic inhomogeneity, the insertion of FM clusters into the metamagnetic matrix. Dc and ac magnetic susceptibilities have been measured, and a magnetic field (*H*) versus temperature (*T*) phase diagram is proposed accordingly. More interestingly, the magnetic phase fractions vary along with the changes in external field and temperature.

[a] College of Chemistry and Molecular Engineering, Beijing National Laboratory for Molecular Sciences, State Key Laboratory for Rare Earth Materials Chemistry and Applications, Peking University,
Beijing 100871, P. R. China
Fax: +86-10-6275-1708
E-mail: jhlin@pku.edu.cn
[b] Department of Physics, Peking University,
Beijing 100871 P. R. China

Supporting information for this article is available on the WWW under http://dx.doi.org/10.1002/ejic.200900387.

Results and Discussions

Structure Description

Compound **1** is isostructural with $M^IM^{III}[BP_2O_7(OH)_3]$ (M^I = Na or K, M^{III} = Al, Ga, In, Fe, V).[4] Crystal data are shown in Table 1. The atomic coordinates, anisotropic displacement parameters, selected bond lengths and angles are given in the Tables 2 and 3. The single-crystal X-ray diffraction study shows that the manganese(III) cations are octahedrally coordinated and the boron/phosphorus atoms

are tetrahedrally coordinated. The selected bond lengths and angles are all in the normal ranges. It should be noted that the MnO_6 octahedron is strongly distorted because of the Jahn–Teller effect in Mn^{III} (d^4). As shown in Figure 1a, there are two long axial Mn–O bonds [2.135(3) Å] and four short Mn–O bonds [1.893(3) and 1.999(3) Å]. This type of tetragonal elongation suggests the electron configuration $t^3{}_{2g}d^1{}_{z2}d^0{}_{x2-y2}$ as in $LiMnO_2$.[5] MnO_6 shares four basal oxygen atoms with PO_4 groups and two other axial corners with BO_4 groups, forming a three-dimensional extended framework, and the backbone of metal ions is therefore a three-dimensional net (see Figures 1b and 1c). The spatial Mn^{3+}–Mn^{3+} distances are approximately 6.1 Å through O–P–O bridges and 5.3 Å through O–B–O bridges. The bond valence sum (BVS) values calculated from the structural parameters are mostly regular (Mn = 3.17, B = 3.07, P = 4.99, O1 = 1.919, O2 = 1.824, O3 = 1.946),[6] while O4 and O5 have significantly low values (1.251 and 1.173), suggesting that additional protons are bonded. The negative charges of the framework are further compensated by the sodium

Table 1. Crystallographic parameters and refinement results for **1**.

Formula	$H_3NaMnBP_2O_{10}$		
CSD number	415996	Z	4
Formula mass	313.70	$\rho_{calcd.}$/g cm^{-3}	2.956
Radiation λ/Å	0.71073	μ(Mo-K_α)/mm^{-1}	2.434
Crystal size/mm	0.3 × 0.3 × 0.4	Refl. collected	654
Morphology	block, black	Independent refl.	621
Space group	$C2/c$	$I > 2\sigma(I)$	601
a/Å	10.504(2)	R_{int}	0.0595
b/Å	8.1747(16)	Refined parameters	72
c/Å	9.0627(18)	θ range/°	3.29–24.94
β/°	115.06(3)°	GOOF	1.000
V/Å^3	704.9(3)	R_1 [$I > 2\sigma(I)$]	0.0694

Table 2. Atomic coordinates and isotropic displacement parameters (in Å^2) for **1**.

Atom	Site	x	y	z	Occupancy	U_{eq}
Mn1	4c	0.2500	0.2500	0.0000	1	0.0280(8)
P1	8f	0.27385(11)	0.06611(13)	0.32079(13)	1	0.0285(8)
O1	8f	0.3185(3)	0.1095(3)	–0.1160(4)	1	0.0322(10)
O2	8f	0.3233(3)	0.0942(4)	0.1875(4)	1	0.0312(10)
O3	8f	0.1131(3)	0.0863(4)	0.2551(4)	1	0.0320(10)
O4	8f	0.3395(3)	0.1917(4)	0.4582(4)	1	0.0326(9)
H4	8f	0.3299	0.2880	0.4306	0.5	0.049
O5	8f	0.0536(3)	0.1239(3)	–0.1023(3)	1	0.0328(10)
H5	8f	–0.0057	0.1637	–0.0763	1	0.049
B1	4e	0.0000	0.0268(8)	–0.2500	1	0.0301(14)
Na	4e	0.5000	–0.1348(3)	0.2500	1	0.0401(9)

Table 3. Selected bond lengths and torsion angles in **1**.

Bond	Length /Å		Angle /°		Angle /°
Mn–O1(×2)	1.893(3)	O1–Mn–O2	89.19(11)	O3–B–O3[a]	103.3(5)
Mn–O2(×2)	1.999(3)	O1–Mn–O2[b]	90.81(11)	O3–B–O5	108.57(16)
Mn–O5(×2)	2.135(3)	O1–Mn–O5	89.46(12)	O3–B–O5[a]	111.15(16)
B–O3(×2)	1.490(5)	O1–Mn–O5[b]	90.54(12)	O3[a]–B–O5	111.15(16)
B–O5(×2)	1.449(4)	O1[b]–Mn–O2[b]	89.19(11)	O3[a]–B–O5[a]	108.57(16)
P–O1	1.543(3)	O1[b]–Mn–O5	90.54(12)	O5–B–O5[a]	113.6(5)
P–O2[c]	1.520(3)	O1[b]–Mn–O5[b]	89.46(12)	O1–P–O2[c]	106.43(17)
P–O3	1.543(3)	O2–Mn–O1[b]	90.81(11)	O1–P–O3	108.86(18)
P–O4	1.534(3)	O2–Mn–O5	90.84(12)	O1–P–O4	111.09(17)
		O2–Mn–O5[b]	89.16(12)	O2[c]–P–O3	111.32(18)
		O2[b]–Mn–O5	89.16(12)	O2[c]–P–O4	110.91(17)
		O2[b]–Mn–O5[b]	90.84(12)	O3–P–O4	106.46(19)
		O2–Mn–O5[b]	89.16(12)	O1–P–O2[c]	106.43(17)

[a] $-x$, y, $-z + 1/2$. [b] $-x + 1/2$, $-y + 1/2$, $-z$. [c] x, $-y$, $z + 1/2$.

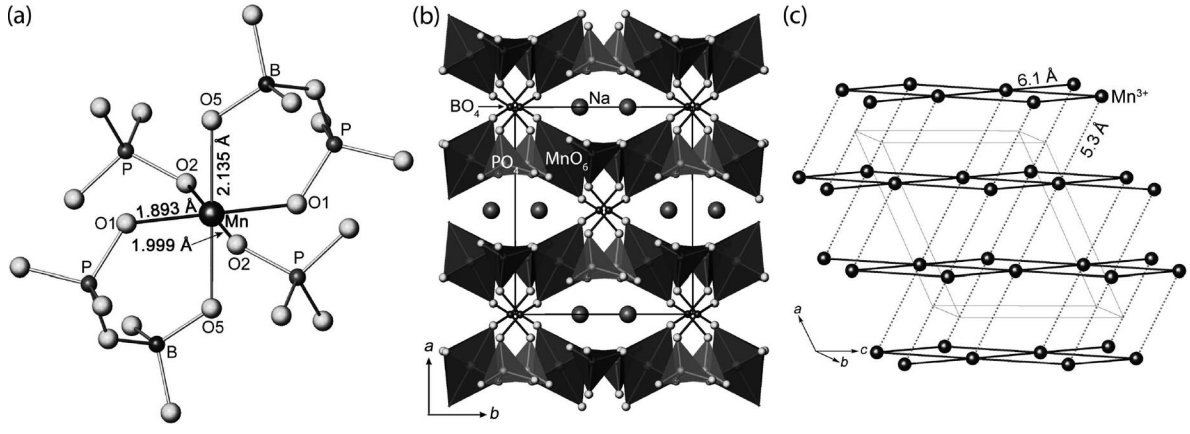

Figure 1. (a) The local coordination environments for Mn, B and P atoms (hydrogen atoms are omitted); (b) the projection along the c axis of the whole structure of **1**; (c) the topology of the Mn^{III} backbone.

cations. The measured atomic ratio for **1** by ICP methods with an ESCALAB2000 analyzer was Na/Mn/B/P ≈ 0.93:1.00:1.02:2.05, which is consistent with the proposed formula. The thermal stability was analyzed by thermogravimetric analysis (TG) with a Dupont 951 Thermogravimetric Analyzer in air with a heating rate of 10 °C/min from 30 to 600 °C. The TG curve shows a one-step mass loss of about 9.6 wt.-%, matching the dehydration of the compound (see Figure S1 in the Supporting Information).

Paramagnetism above 10 K

The temperature- and field-dependent magnetization in both dc and ac were performed in order to have a clear view of the magnetism of **1**. In the high-temperature region, the title compound shows a typical paramagnetism. For instance, the temperature-dependent susceptibility ($\chi = M/H$) above 30 K gives a very good Curie–Weiss fit (see the inset of Figure 2a). The obtained Curie constant (C = 3.00 $cm^3 mol^{-1} K$) agrees well with the theoretical value of the isolated high spin Mn^{III} (3.0 $cm^3 mol^{-1} K$ for $S = 2$). The positive Weiss temperature (θ = 13.3 K) suggests that the predominant interaction among Mn^{III} is ferromagnetic (FM) at high temperature, which can also be visualized by a sharp increase in χT (vs. T) in going from 20 K to 10 K. As already stated in the Introduction, compound **1** processes a complex magnetism at low temperature, namely magnetic inhomogeneity, which is composed of ferromagnetic clusters and a metamagnetic background. Details for different temperature ranges will be shown in the following sections.

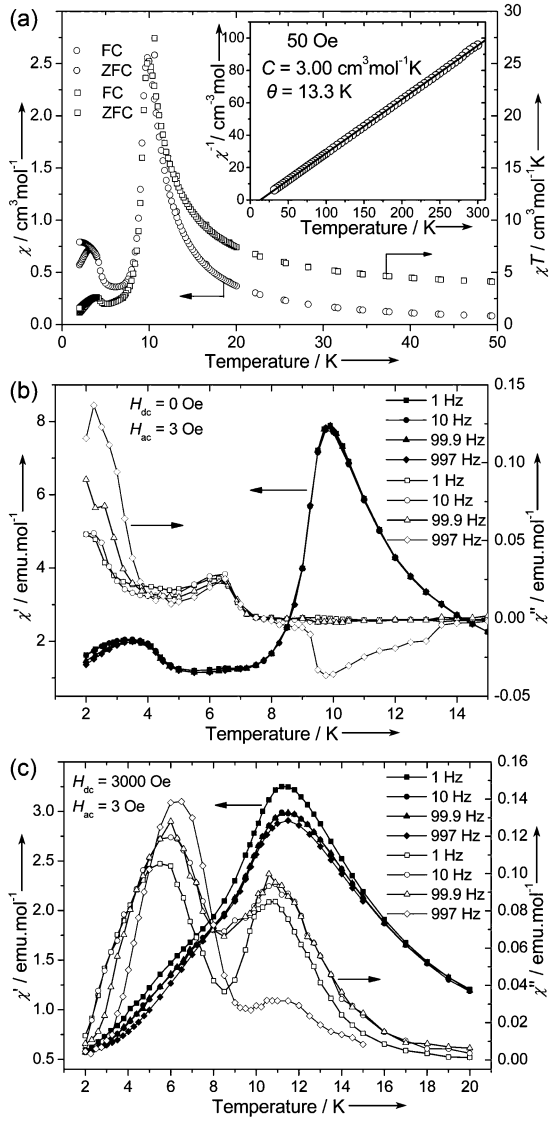

Figure 2. (a) The plots of χ and χT vs. T at 50 Oe. The inset is the Curie–Weiss fit of the data above 30 K; (b) and (c) temperature dependence of the ac susceptibility (χ', in-phase signals; χ'', out-of-phase signals) at frequencies of 1 (■/□), 10 (●/○), 99.9 (▲/△) and 997 Hz (♦/✧).

Metamagnetism between 6.5 K and 10 K

10 K is the first critical transition temperature. As shown in Figure 2a, the low-field χ curve shows a pronounced peak at approximately 10 K. Below 10 K, the susceptibility decreases rapidly and reaches a minimum at approximately 6 K. All these indicate that the magnetic ordering state at approximately 10 K and 50 Oe field is antiferromagnetic (AFM), irrespective of the predominant FM interaction. On the other hand, the isothermal magnetization curves at 7–9 K have a sigmoidal shape (see Figure 3), which points out that **1** is a metamagnet at this temperature region, and the critical field is approximately 550 Oe as estimated from dM/dH curves (see the inset of Figure 3).

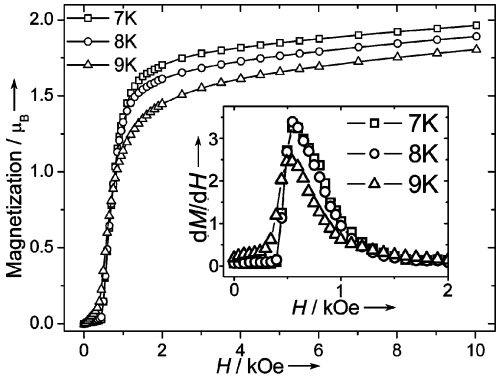

Figure 3. Isothermal magnetization curves at 7, 8 and 9 K. The insets are the dM/dH plots.

Such metamagnetism is also confirmed by ac susceptibility measurements (see Figure 2b and Figure 2c): when H_{dc} = 0, only χ' shows a peak at approximately 10 K; while both χ' and χ'' have peaks at around 11 K when H_{dc} = 3 kOe. This means that the AFM ordering at 0 Oe changes to a FM ordering at 3 kOe. For simplicity, we define the state at low field as AFM and the high-field state as FM.

A Ferromagnetic Cluster Inserted in a Metamagnetic Background between 3.5 K and 6.5 K

From the peak distinguished at 6.5 K in the χ'' curve without static field (see Figure 2b), it is known that 6.5 K is the second key point. Ideally, there should also be a peak at this temperature in the real susceptibility curve. However, it is absent in our curve. The reason is probably that this peak is suppressed in magnitude by the two peaks nearby. In fact, we do see a tiny non-flat anomaly (or tendency to be a peak) here in the real susceptibility curve.

The appearance of a peak in the imaginary susceptibility curve always suggests spontaneous magnetism, which means that the transition at 6.5 K is ferromagnetic in nature. However, there are no hysteresis loops in the isothermal magnetization curves at 4–6 K (see Figure 4), which show the same sigmoidal shape as those at 7–9 K, indicating metamagnetism. This looks like a contradiction.

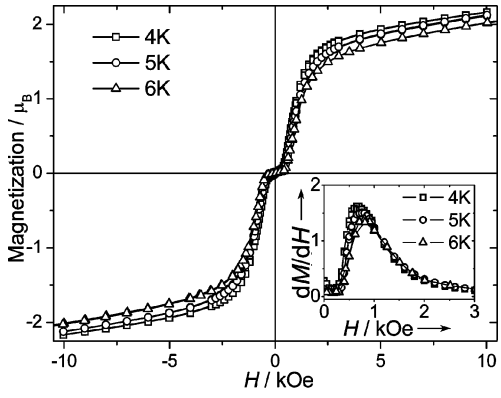

Figure 4. Isothermal magnetization curves at 4, 5 and 6 K. The insets are the dM/dH plots.

In fact, the dc susceptibility curve at 50 Oe has a kink at 6 K and turns upwards thereafter, which is a sign of ferromagnetism. Field cooling (FC) and zero field cooling (ZFC) curves display a bifurcation at approximately 3.5 K. Moreover, the ZFC curve exhibits a decrease below approximately 3.5 K, which is a typical sign of spin glass or cluster glass magnets.[7] Considering all the above phenomena, the plausible contradiction we mentioned above could be explained by using a model of magnetic inhomogeneity composed of ferromagnetic clusters and a metamagnetic background. The transition temperature of 6.5 K is assigned as the Curie-like temperature T_c,[8] where a set of ferromagnetic clusters is formed due to short-range ordering defined as ferromagnetic cluster (FMC) for simplicity. In literature, the typical diameter of such kinds of clusters is approximately 10 Å (like in La-doped $CaMnO_3$).[3] So, it should be noted that this so-called Curie-like temperature does not represent a true long-range ordering, because the spatial fraction of the FMC is too small to coalesce as a homogeneous magnet. In such a scenario, there will be no hysteresis loops because it is just a short-range ferromagnetic ordering. So, the M–H curves at 4–6 K only represent the behaviour of the major phase, which is the metamagnetic background. In addition, the peak at 6.5 K ought to be sensitive to different frequencies because of the short-range ordering, which is exactly the case in **1** (see Figure 2b). Now that **1** has been shown to contain ferromagnetic clusters, then it is reasonable to assume that these clusters could be frozen at lower temperature (at low external field). Accordingly, the peak at approximately 3.5 K in the ac susceptibility curve corresponds to this frozen cluster phenomenon.

The isothermal magnetizations at 4–6 K are presented in Figure 4, which shows a classical metamagnetism. No hysteresis loop is detected. The critical fields are 800 (6 K), 750 (5 K), 700 Oe (4 K). It is worthy of note that the critical fields show an abrupt jump around 6.5 K (from 550 Oe at 7 K to 800 Oe at 6 K), which is the ordering temperature of the FMC. This is strong evidence that the different magnetic states are strongly related. As a result, we can preclude the possibility that the metamagnetic and ferromagnetic cluster phases are compositionally segregated. Only when the clusters are inserted into the metamagnetic domains would the critical field needed for the transition from AFM to FM be affected by the appearance of the short-range ordering of the FMC. On the other hand, the decreasing tendency of critical fields from 6 K to 4 K is possibly due to the diminishing of the metamagnetic component. It is also well known that different phase fractions in Mn perovskites could vary the relative ratio with decreasing temperature.[3a]

Figure 2c also shows the ac susceptibility at a relatively high field (3 kOe), where two distinct and frequency-dependent peaks are observed at approximately 6.5 K and 11 K. We know that the FM ordering occurring at approximately 11 K is derived from the AFM state of the metamagnetic background. The second peak appearing at approximately 6.5 K is related to the short-range ordering of the FMC. In contrast to the zero field data in Figure 2b, there is no freezing point at 3 kOe, because the high magnetic field will break the frozen characteristic of the cluster glass.

Since there are two peaks in Figure 2c related to the phase transitions of two different magnetic phases, it is easy to understand that the spin configurations of the FM and FMC phases are intrinsically different, although they are both ferromagnetic in nature. According to the crystal structure, there are two superexchange pathways through three-atom bridges, i.e. the O–P–O and O–B–O bridges. Empirically, if these two magnetic pathways mediate different types of exchange interactions, the strong one is FM and the weak one is AFM in nature (the predominant exchange should be FM because of the positive θ value), the title compound would show metamagnetism as it is, either in a one-dimensional model (while the O–B–O bridges carry the FM interactions) or in a two-dimensional model (while the O–P–O bridges carry the FM interactions). We cannot tell which model it would be and cannot present the magnetic structures of these two ferromagnetic phases on the basis of the present experimental results alone. We believe that the long-range ordering of the metamagnetic background phase is triggered by these two superexchange interactions. Differently, the appearance of the ferromagnetic cluster phase is then supposed to be conducted by

another factor. Note that Mn^{III} associated with d^4 electron configuration has an appealing magnetic peculiarity (large magnetic anisotropy), which usually plays a key role in constructing single-molecule magnets[9] (Mn_{12}, Mn_{25}, Mn_{85}) and single-chain magnets[10] (Mn^{III}–Ni^{II}). Herein, the Mn^{III} ions in **1** also show a strong Jahn–Teller effect, and the MnO_6 octahedra are tetragonally elongated, which suggests the large anisotropic character of Mn^{III}. So, we propose a possibility that the ferromagnetic cluster phase is formed mainly as a result of the large magnetic anisotropy. In summary, the origins of these two magnetic phases (FM and FMC) could be different, which show competition at low temperature probably due to the comparative potential energies of the two phases.

In comparison with the zero field ac susceptibility, the comparative intensity of the peak at 6.5 K is significantly enhanced at 3 kOe, which suggests that the spatial ratio of FMC/FM increases under higher magnetic field. It is very reminiscent of the inhomogeneous magnetism in electron-doped Mn perovskites, where the relative phase fractions could also be influenced by different external applied magnetic fields.[2e] Both peaks (6.5 K and 11 K) in the ac curves at 3 kOe show significant frequency dependence, which means that the FM and FMC states are both short-range ordering states under this condition. It makes sense that the ordering of the FM phase changes from a nearly long-range ordering at zero field to a short-range ordering at 3 kOe, as the spatial ratio of the FMC phase increases with the enhanced field. This phenomenon can be explained by the fact that the relative potential energies of the two phases can be adjusted by magnetic fields because of their different origins, and apparently, the FMC phase is favourable at high field.

Ferromagnetic Cluster Glass and Metamagnetic Background below 3.5 K

Below 3.5 K, the FMC state transfers to its glassy version (designated as FMCG) at low field. The isothermal magnetization curves from 2.8 K to 2 K can be well explained by the magnetic inhomogeneity theory (see Figure 5). Here, we introduce the magnetization process at 2.4 K as being representative (see Figure 5c). The initial magnetization first increases slowly and linearly up to 400 Oe, and it then increases rapidly. The change in slope includes two contents: one is the transition of the metamagnetic background from the AFM to the FM state and the other is the melting of the FMCG state. After high-field magnetization, the following demagnetization process shows a finite magnetic remanence (0.33 μ_B) and a small coercive field (38 Oe). The remanence originates from the FMCG component, because the clusters tend to be frozen at low field and could partially retain the high-field mag-

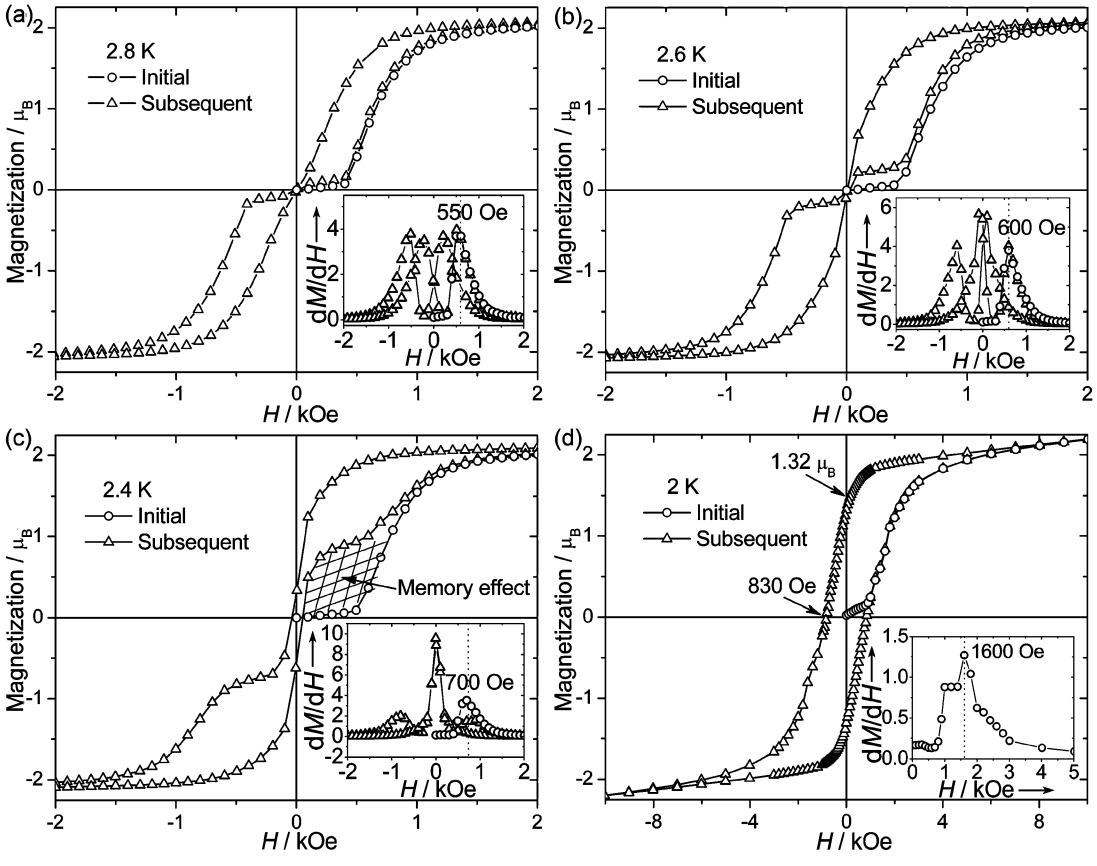

Figure 5. Isothermal magnetization curves. The insets are the dM/dH plots.

netized ferromagnetic spin arrangement. With further enhancement of the field in the negative direction, the magnetization first shows a rapid increase from –38 Oe to –200 Oe, which is different from what happened at the initial magnetization process. This rapid magnetization is also related to the FMCG, which now remains partially in ferromagnetic ordering after high-field magnetization and behaves like a ferromagnet. From –200 Oe and –400 Oe, the magnetization shows a linear and slow increase period again, which is attributed to the metamagnetic phase. The second magnetization curve in the positive direction is different from the first one. It shows a so-called memory effect.

As shown in Figure 5, the values of the remanence and coercive field increase from 2.8 K to 2.4 K, indicating that the FMCG phase develops with decreasing temperature. The isothermal magnetization at 2 K shows a slight difference: there is no linear part any more in the second magnetization process (see Figure 5d). It does not necessarily mean that there is no metamagnetic phase below 2 K. The disappearance of the linear part in magnetization at 2 K is probably due to the very large remanence (1.32 μ_B) and coercive field (830 Oe), which can "swallow" the metamagnetic transition.

Conclusions

By combining dc and ac magnetic measurements, one may construct a magnetic phase diagram for **1** (see Figure 6). There are six boundaries: I is the temperature-induced AFM or FM ordering transition of the metamagnetic background; II is the field-induced metamagnetic transition; III is the short-range ordering transition of the FMC component. It may not be a straight line; however, we just obtained two critical points at low and high fields so far; the meaning of IV is the same as II, but the values of critical fields are obviously higher because of the influence of the short-range ordered FMC component; V is the frozen line of the FMC component; VI is slightly different from V and means not only the frozen line of the FMC but also the AFM–FM transition of the background phase.

The magnetic behaviour of **1** is very complex because of the inhomogeneity. Similar phenomena are extensively observed in perovskite manganites, in which the physical mechanism is the competition between ferromagnetic DE (Mn^{III}–O–Mn^{IV}) and antiferromagnetic SE (Mn^{III}–O–Mn^{III}) interactions.[2] However, the same mechanism might not work in $NaMn^{III}[BP_2O_7(OH)_3]$, because there is no evidence for the coexistence of Mn^{III} and Mn^{IV} in **1**, and the magnetic couplings here are conducted by three-atom bridges (i.e. O–B–O or O–P–O), not the oxygen atom only. In addition, the magnetic inhomogeneity in **1** is also different from that in perovskite manganites, where the inhomogeneity contains FM clusters and an antiferromagnetic background.

At present, the origin of magnetic inhomogeneity in **1** still remains open. It is well known that the magnetic inhomogeneity is normally a consequence of competition. Herein, the Mn^{III} ions in **1** show a strong Jahn–Teller effect. So we propose a clue that the competition in **1** is possibly between the magnetic superexchange interactions and the large magnetic anisotropy. Further investigation is needed, and the magnetotransport property of **1** is also of potential interest under the consideration of this unusual inhomogeneous mechanism.

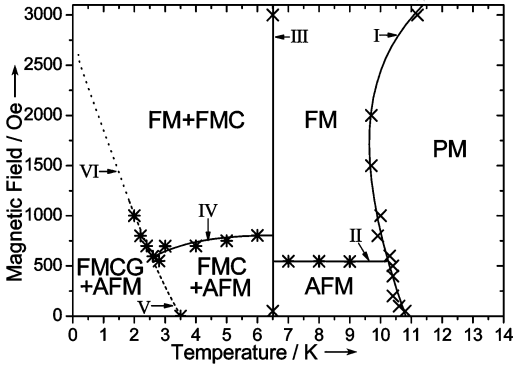

Figure 6. *H*–*T* magnetic phase diagram for **1**. The boundary shown by short dotted lines is not determined by experiment but just assumed to guide the eye. The critical points between paramagnetic (PM) and AFM (or FM) states are estimated form $d(\chi T)/dT$ values measured at different external fields (see Figures S2 and S3 in the Supporting Information).

Experimental Section

All reagents were of analytical grade and were used as obtained from commercial sources without further purification. Typically, a mixture of MnO_2 (5 mmol), $Na_2B_4O_7{\cdot}10H_2O$ (10 mmol) and concentrated H_3PO_3 (3 mL, 14.6 mol/L) was charged into a 50 mL Teflon reactor and heated at 200 °C in a steel autoclave for 4 d. The solid product was washed extensively with hot water (80 °C) until the soluble components were completely removed. Black block single crystals of **1** were obtained with a yield of about 95% based on metal resource.

A single crystal of about $0.3 \times 0.3 \times 0.4\ mm^3$ was used for X-ray diffraction data collection at room temperature by using a Rigaku AFC6S diffractometer with graphite-monochromated Mo-K_α radiation (λ = 0.71073 Å) by the ω-2θ scan method. The structure was solved with direct methods and refined on F^2 by full-matrix least-squares methods with the programs SHELXS-97 and SHELXL-97.[11] All non-hydrogen atoms were refined anisotropically by a full-matrix least-squares technique. Further details of the crystal structure investigation may be obtained from the Fachinformationszentrum Karlsruhe, 76344 Eggenstein-Leopoldshafen, Germany [Fax: +49-7247-808-666; E-mail: crysdata@fiz-karlsruhe.de], on quoting the depository number CSD-415996.

The magnetic properties were investigated with a Quantum Design MPMS-SS superconducting quantum interference device (SQUID) magnetometer. For measuring the magnetic susceptibility, crystals of **1** were placed in a gelatine capsule fastened in a plastic straw for immersion into the SQUID. For a typical ZFC measurement, we cooled the system to 2 K without the external field, then applied a setting magnetic field, and the magnetization was measured in the following warming process. After that, we cooled the system again and measured the FC magnetization in the meanwhile. When

different fields were employed, we increased the temperature of the system to 20 K after every thermal cycle to avoid the magnetic hysteresis effect.

Supporting Information (see footnote on the first page of this article): TG, IR, χ–T, M–T and M–H curves at different temperatures.

Acknowledgments

We thank Prof. Jirong Sun (Chinese Academy of Sciences), Prof. Song Gao (Peking University) and Dr. Jing Ju (Tohoku University) for helpful discussions on magnetism. We thank Dr. Guobao Li (Peking University) for the collection of single-crystal X-ray diffraction data and Ms. Fuhui Liao (Peking University) for TGA measurements. This work was supported by the Nature Science Foundation of China.

[1] E. Dagotto, *Science* **2005**, *309*, 257–262.

[2] a) C. Martin, A. Maignan, M. Hervieu, B. Raveau, *Phys. Rev. B* **1999**, *60*, 12191–12199; b) J. J. Neumeier, J. L. Cohn, *Phys. Rev. B* **2000**, *61*, 14319–14322; c) J. Alonso, E. Herrero, J. M. González-Calbet, M. Vallet-Regí, J. L. Martinez, J. M. Rojo, A. Hernando, *Phys. Rev. B* **2000**, *62*, 11328–11331; d) M. Respaud, J. M. Broto, H. Rakoto, J. Vanacken, P. Wagner, C. Martin, A. Maignan, B. Raveau, *Phys. Rev. B* **2001**, *63*, 144426; e) P. A. Algarabel, J. M. De Teresa, B. García-Landa, L. Morellon, M. R. Ibarra, C. Ritter, R. Mahendiran, A. Maignan, M. Hervieu, C. Martin, B. Raveau, A. Kurbakov, V. Trounov, *Phys. Rev. B* **2002**, *65*, 104437; f) J. Burgy, M. Mayr, V. Martin-Mayor, A. Moreo, E. Dagotto, *Phys. Rev. Lett.* **2001**, *87*, 277202; g) C. Chiorescu, J. J. Neumeier, J. L. Cohn, *Phys. Rev. B* **2006**, *73*, 014406; h) C. Sen, G. Alvarez, E. Dagotto, *Phys. Rev. Lett.* **2007**, *98*, 127202; i) R. Cortés-Gil, J. M. Alonso, M. L. Ruiz-González, M. Vallet-Regí, A. Hernando, J. M. González-Calbet, *Chem. Mater.* **2008**, *20*, 3398–3403.

[3] a) C. D. Ling, E. Granado, J. J. Neumeier, J. W. Lynn, D. N. Argyriou, *Phys. Rev. B* **2003**, *68*, 134439; b) E. Granado, C. D. Ling, J. J. Neumeier, J. W. Lynn, D. N. Argyriou, *Phys. Rev. B* **2003**, *68*, 134440 and the reference cited therein.

[4] a) I. Boy, G. Cordier, B. Eisenmann, R. Kniep, *Z. Naturforsch., Teil B* **1998**, *53*, 165–170; b) D. Koch, R. Kniep, *Z. Kristallogr. New Cryst. Struct.* **1999**, *214*, 441–442; c) Y. X. Huang, S. Y. Mao, J. X. Mi, Z. B. Wei, J. T. Zhao, R. Kniep, *Z. Kristallogr. New Cryst. Struct.* **2001**, *216*, 15–16; d) Y. X. Huang, J. X. Mi, S. Y. Mao, Z. B. Wei, J. T. Zhao, R. Kniep, *Z. Kristallogr. New Cryst. Struct.* **2002**, *217*, 7–8; e) L. R. Zhang, H. Zhang, H. Borrmann, R. Kniep, *Z. Kristallogr. NCS.* **2002**, *217*, 477–478; f) J. X. Mi, Y. X. Huang, S. Y. Mao, H. Borrmann, J. T. Zhao, R. Kniep, *Z. Kristallogr. New Cryst. Struct.* **2002**, *217*, 167–168.

[5] a) J. E. Greedan, N. P. Raju, I. J. Davidson, *J. Solid State Chem.* **1997**, *128*, 209–214; b) D. G. Kellerman, J. E. Medvedeva, V. S. Gorshkov, A. I. Kurbakov, V. G. Zubkov, A. P. Tyutyunnik, V. A. Trunov, *Solid State Sci.* **2007**, *9*, 196–204.

[6] I. D. Brown, D. Altermatt, *Acta Crystallogr., Sect. B* **1985**, *41*, 244–247.

[7] a) J. W. Cai, C. Wang, B. G. Shen, J. G. Zhao, W. S. Zhan, *Appl. Phys. Lett.* **1997**, *71*, 1727–1729; b) D. D. Stauffer, C. Leighton, *Phys. Rev. B* **2004**, *70*, 214414; c) S. Karmakar, S. Taran, B. K. Chaudhuri, H. Sakata, C. P. Sun, C. L. Huang, H. D. Yang, *Phys. Rev. B* **2006**, *74*, 104407.

[8] X. Y. Zhang, Y. Chen, Z. Y. Li, G. Vittoria, V. G. Harris, *J. Phys.: Condens. Matter* **2007**, *19*, 266211.

[9] a) A. Caneschi, D. Gatteschi, R. Sessoli, A. L. Barra, L. C. Brunel, M. Guillot, *J. Am. Chem. Soc.* **1991**, *113*, 5873–5874; b) R. Sessoli, D. Gatteschi, A. Caneschi, M. A. Novak, *Nature* **1993**, *365*, 141–143; c) R. Sessoli, H. L. Tsai, A. R. Schake, S. Y. Wang, J. B. Vincent, K. Folting, D. Gatteschi, G. Christou, D. N. Hendrickson, *J. Am. Chem. Soc.* **1993**, *115*, 1804–1816; d) M. Murugesu, M. Habrych, W. Wernsdorfer, K. A. Abboud, G. Christou, *J. Am. Chem. Soc.* **2004**, *126*, 4766–4767; e) A. J. Tasiopoulos, A. Vinslava, W. Wernsdorfer, K. A. Abboud, G. Christou, *Angew. Chem. Int. Ed.* **2004**, *43*, 2117–2121.

[10] R. Clérac, H. Miyasaka, M. Yamashita, C. Coulon, *J. Am. Chem. Soc.* **2002**, *124*, 12837–12844.

[11] G. M. Sheldrick, *SHELXS 97, Program for the Solution of Crystal Structures*, University of Göttingen, Göttingen, Germany, **1997**. G. M. Sheldrick, *SHELXL 97, Program for the Refinement of Crystal Structures*, University of Göttingen, Göttingen, Germany, **1997**.

Received: April 28, 2009
Published Online: July 27, 2009

